39th IAHR WORLD CONGRESS
GRANADA, SPAIN 2022
From Snow to Sea
19-24 June 2022

Proceedings of the 39th IAHR World Congress
19-24 June 2022
Granada, Spain
DOI number

Comparison of Signal Processing Algorithms for Multi-Sensor Intrusive Phase-Detection Probes

Matthias Bürgler[(1)], Benjamin Hohermuth[(1)], David F. Vetsch[(1)] and Robert M. Boes[(1)]

[(1)]Laboratory of Hydraulics, Hydrology and Glaciology (VAW), ETH Zurich, Zurich, Switzerland
buergler@vaw.baug.ethz.ch, hohermuth@vaw.baug.ethz.ch, vetsch@vaw.baug.ethz.ch, boes@vaw.baug.ethz.ch

Abstract

Measurements of two-phase flow properties in highly turbulent, self-aerated free-surface flows remain a challenging task. The combination of dual-tip intrusive phase-detection probes with the recently developed adaptive window cross-correlation (AWCC) signal processing allows for measurements of local pseudo-instantaneous 1-D velocities. However, the applied window averaging reduces the data rate and thereby limits the retrieval of time-resolving turbulence statistics. Nevertheless, this represents the best practice in the field of hydraulic engineering. Meanwhile, intrusive phase-detection probes with more than two sensors are well-established in nuclear and chemical engineering. The use of four or more probe tips in combination with suitable signal processing algorithms enables the measurement of local instantaneous 3-D particle velocity vectors and particle diameters. The applied signal processing algorithms are typically based on event-detection and thus yield an increased data rate in comparison to the AWCC approach. In this work, we compare two signal processing algorithms for multi-sensor intrusive phase-detection probes and evaluate their applicability for measurements of two-phase flow properties in highly turbulent free-surface flows. A dual-tip intrusive phase-detection probe in combination with the AWCC technique serves as a benchmark. To this end, we use synthetically generated particle velocity time series, which are obtained by modeling bubble trajectories based on synthetic stochastic velocity fields. This approach is advantageous over experimentally obtained signals in that the true instantaneous velocities and particle shapes are known, allowing for a direct comparison of the signal processing algorithms. Furthermore, we discuss the limitations of the considered signal processing algorithms and highlight future research opportunities.

Keywords: Aerated flow; Two-phase flow turbulence; Conductivity probe; Signal processing; Stochastic simulation

1. INTRODUCTION

Spillways are important safety elements of reservoir dams and are designed to safely convey excess water during extreme floods. The acceleration of the water along the spillway results in the formation of a turbulent boundary layer (Bauer, 1954; Castro-Orgaz and Hager, 2010). The thickness of the turbulent boundary layer increases until the upper edge intersects with the free surface, given that the spillway is sufficiently long. The intersection of the turbulent boundary layer with the free surface is often associated with the onset of air entrainment (e.g., Wood, 1991). High turbulence levels cause air transport in vertical direction towards the spillway invert, resulting in S-shaped air concentration distributions over the flow depth (Straub and Anderson, 1958). The resulting air-water flow mixture exhibits significantly altered depth-averaged velocity, flow depth and turbulence statistics compared to single-phase flow (e.g., Chanson, 1994, 1997).

A detailed physical description of such highly turbulent, self-aerated free-surface flows is essential for the safe design of many types of hydraulic structures, such as spillways and low-level outlets. The measurement of flow properties in prototypes is cumbersome due to difficulty of access and uncontrollably violent flow conditions. Therefore, laboratory-scale models are typically used for the investigation of high-velocity air-water flows. Instrumentation for flow properties in the non-aerated single-phase flow region, such as mechanical (Pitot tubes), acoustic (ADV) and optical techniques (LDA, PIV), are well advanced (Aberle et al., 2017) and therefore, depths, flow velocities, as well as boundary layer development in the non-aerated region of spillways are well described (e.g., Bauer, 1954; Wood, 1991). However, when air concentrations exceed about 1-3%, the application of the same instrumentation becomes less reliable (Chanson, 2013). Instead, dual-tip intrusive phase-detection probes in combination with cross-correlation based signal processing have been the preferred method over several decades for the retrieval of time averaged velocities (Neal and Bankoff, 1963; Wood, 1983) and other air-water flow properties including void fraction, particle frequencies and particle chord lengths (Straub and Anderson, 1958; Boes and Hager, 2003; Felder and Chanson, 2014). The recently proposed adaptive window cross-correlation (AWCC) signal processing algorithm (Kramer et al., 2019, 2020a) allows for robust

measurements of local pseudo-instantaneous 1-D velocities of signal windows consisting of a discrete number of particles N_p (bubbles or droplets) and significantly improved measurement accuracy of turbulent statistics in highly aerated flows compared to previous methods (Chanson and Toombes, 2002). However, the applied window averaging still reduces the data rate in comparison to event-detection algorithms (Kramer et al., 2020b), thereby introducing an averaging effect on turbulence quantities and limiting the retrieval of time-resolving turbulence statistics. While Kramer et al. (2020a) proposed a method to overcome the smoothing effect as a result of window averaging by extrapolation of turbulence levels to N_p = 1, this approach requires calibration. In any case, information from dual-tip probes is limited to streamwise velocities, prohibiting the measurement of vertical velocity fluctuations which are of special interest in the context of air-water flows. In addition, vertical and transverse velocity fluctuations may lead to a bias of pseudo-instantaneous streamwise velocity measurements as any change in travel time is interpreted as streamwise fluctuation (Hohermuth et al., 2021).

In related research fields of nuclear and chemical engineering, intrusive phase-detection probes with four sensors are frequently applied in bubbly flows and different signal processing algorithms have been proposed to reconstruct local instantaneous 3-D particle velocity vectors, particle diameters and interfacial area concentrations (e.g., Shen et al., 2005; Shen and Nakamura, 2014; Tian et al., 2015). The algorithms proposed by Shen and Nakamura (2014) and Tian et al. (2015) are based on particle event detection and thus yield an increased data rate in comparison to the AWCC approach. Additionally, measurements of local instantaneous 3-D particle velocity time series enable the retrieval of the full Reynolds stress tensor. Therefore, the application of four-sensor probes with appropriate signal processing algorithms could provide relevant insight on boundary layer development, 3-D turbulence statistics and improve our understanding of air entrainment and transport processes at hydraulic structures.

The approaches of Shen and Nakamura (2014) and Tian et al. (2015) were successfully validated in bubbly flows, i.e., flows with relatively low void fractions and large bubbles, but their robustness in high-velocity flows with high air concentrations and smaller particle diameters has not yet been tested. Therefore, we compare the signal processing algorithms of Shen and Nakamura (2014) and Tian et al. (2015) for a four-sensor intrusive phase-detection probe and evaluate their applicability for measurements of two-phase flow properties in turbulent high-velocity free-surface flows. To this end, we use synthetically generated signal time series, by modeling 3-D bubble trajectories based on stochastic velocity time series. Further, we use a dual-tip intrusive phase-detection probe in combination with the AWCC technique as a benchmark.

2. METHODS

Synthetically generated signal times series have been used to test air-water flow instrumentation in recent studies (e.g., Kramer et al., 2019, 2020a; Valero et al., 2019). Herein, we extend these approaches to 3-D velocity fields with correlations between stream- and spanwise components to model shearing. In addition, the dispersed-phase movement was not assumed to directly follow the fluid velocity field but was derived from a force balance equation (Fig. 1).

The required input parameters of the fluid flow field include the time averaged velocity $\bar{u}_{f,i}$ with the subscripts f and i denoting the fluid phase and spatial dimensions ($i = x, y, z$), respectively, the turbulent intensity $T_{I,i}$, the integral time scale $T_{L,i}$, the realization frequency f_r, at which time series values are generated, and the duration of the time series t_s. Further required parameters of the dispersed phase are the mean bubble diameter d_b, the standard deviation σ characterizing the log-normal distribution of the bubble diameters, and the air concentration C_a. The synthetic phase-detection probe signals are then generated by tracking the bubble movement with respect to the probe sensors, which requires the location $p_{i,j}$ of each sensor j as well as the sampling frequency f_s of the probe. Finally, the signal processing algorithms are applied to obtain the reconstructed velocity time series.

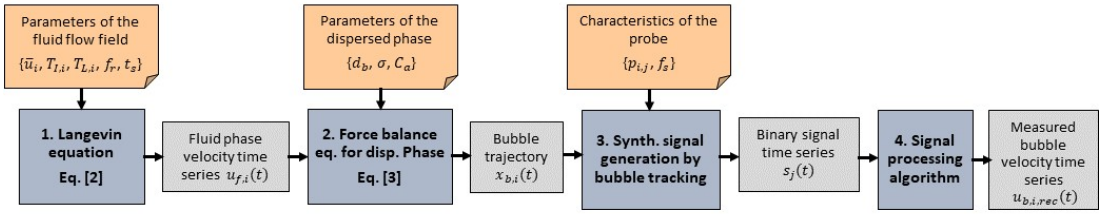

Figure 1. Workflow to compare signal processing algorithms based on synthetically generated signals of virtual phase-detection probes.

2.1 Stochastic Velocity Time Series

Let u_i be the instantaneous velocity. The decomposition of the instantaneous velocity into a time averaged $\bar{u}_i$ and a fluctuation part u_i', respectively, is given by Eq. [1].

$$u_i = \bar{u}_i + u_i' \quad [1]$$

In a first step, a stochastic time series for the fluid phase (water) $u_{f,i}(t)$ with duration t_s is generated with the Langevin equation in finite difference form (Pope, 2000) in Eq. [2], where $\Delta t_1 = 1/f_r$ denotes the discrete time step, $u'_{f,i,rms}$ the root mean square (RMS) velocity fluctuation and $\xi(t)$ is a standardized Gaussian random variable (N(0,1)).

$$u_{f,i}(t+\Delta t_1) = \bar{u}_{f,i} + \left(u'_{f,i}(t) - \bar{u}_{f,i}\right)\left(1 - \frac{\Delta t_1}{T_{L,i}}\right) + u'_{f,i,rms}\sqrt{\left(\frac{2\Delta t_1}{T_{L,i}}\right)}\,\xi(t) \quad [2]$$

While it is reasonable to assume that entrained air bubbles are transported at almost identical mean velocities as the fluid (Chanson, 1997), significant phase-slip may occur at small time scales, resulting in a damping of the turbulent fluctuations due to added mass and Basset forces (Crowe et al., 1998). Balachandar and Eaton (2010) provide a semi-empirical balance of forces acting on dispersed particles in uniform flow. To obtain a velocity time series $u_{b,i}(t)$ for entrained air bubbles (subscript b) with a mean diameter d_b, we integrate a simplified force balance equation for particles given in Eq. [3], accounting for drag and added mass forces of the fluid while using a first order Euler scheme. In Eq. [3], V_b is the bubble volume, ρ_b and ρ_f are the bubble and fluid density, respectively, $C_M = 0.5$ is the added mass coefficient, and C_d is the drag coefficient. The drag coefficient is calculated as $C_d = 24/Re_b(1 + 0.15(Re_b)^{0.687})$ (Tomiyama et al., 1998), where $Re_b = \left(|u_{f,i} - u_{b,i}|\right)d_b/\nu_f$ is the particle Reynolds number and ν_f the kinematic fluid viscosity.

$$V_b\left(\rho_b + C_M\rho_f\right)\frac{du_{b,i}}{dt} = \frac{1}{2}\frac{\pi}{4}d_b\left(u_{f,i} - u_{b,i}\right)|u_{f,i} - u_{b,i}|\rho_f C_d \quad [3]$$

Based on the stochastic velocity time series of the dispersed phase, the dispersed phase trajectory is calculated by semi-implicit integration of the velocity time series as described by Eq. [4], where $x_{b,i}$ denotes the location with regards to the ith spatial dimension and $\Delta t_1 = 1/f_r$.

$$x_{b,i}(t+\Delta t_1) = x_{b,i}(t) + \left(\frac{u_{b,i}(t) + u_{b,i}(t+\Delta t_1)}{2}\right)\Delta t_1 \quad [4]$$

In Figure 2a, an exemplary stochastic velocity time series of the fluid and the dispersed air phase (bubbles) are illustrated, while the corresponding power spectral densities (PSD) estimated with the Welch's method (Welch, 1967) are shown in Figure 2b.

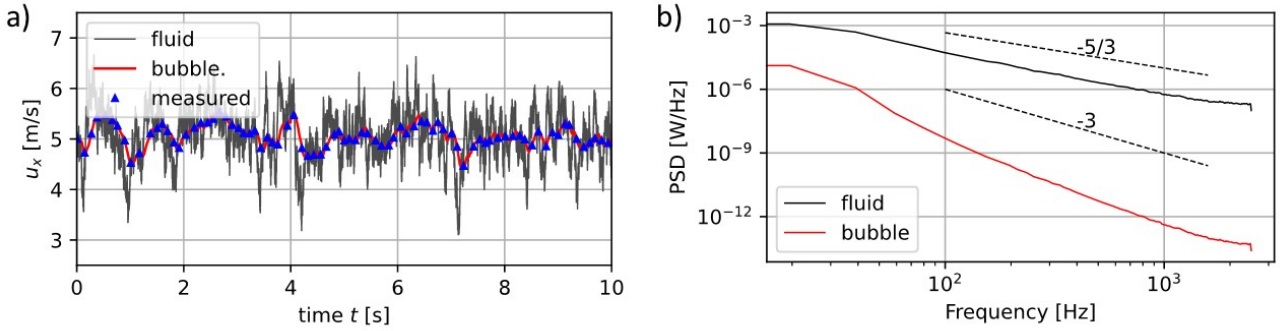

Figure 2. Exemplary synthetic and measured velocity time series a) of the fluid and bubbles and b) the corresponding power spectral densities (PSD) of the stochastic time series.

2.2 Synthetic Signal Generation

A finite number of bubbles is defined as $N_b = F \cdot t_s$, where t_s is the duration of the stochastic time series and $F = 1.5\,C_a|\bar{u}_b|/d_b$ is the bubble count rate, with C_a being the air concentration and $|\bar{u}_b|$ the magnitude of the time averaged bubble velocity, respectively. The individual bubble diameters are sampled from a lognormal

distribution $d_{b,k}$~LN(μ, σ^2). The parameter $\mu = \ln(d_b) - 0.5\sigma^2$ is calculated from an expected value of the bubble diameter. Based on measured bubble size distribution on stepped spillways (Kramer, 2019), a value of 1.3 is adopted for the scaling parameter σ.

Instead of simulating a 1-D stream of bubbles that are perfectly aligned with the probe tips (Kramer et al., 2019), we adopt a slightly different approach to account for off-centerline piercing of bubbles. For each bubble k, an arrival time $t_{a,k}$ and a corresponding arrival location $x_{b,i}(t_{a,k})$ are defined based on equal interarrival times $t_{iat} = t_s/N_b$. The interaction of each bubble k with the virtual phase-detection probe is then simulated by placing the probe's yz-plane centroid with an offset ε_i compared to the arrival location $(x_{b,i}(t_{a,k}))$ at $c_{p,i,k} = x_{b,i}(t_{a,k}) + \varepsilon_{i,k}$ and tracking the bubble movement along the trajectory. Assuming that the main flow direction is aligned with the probe and the x-axis results in $\varepsilon_x = 0$ and off-centerline piercing of bubbles is simulated by sampling the offsets ε_y and ε_z uniformly at random ε_i~U$(-\frac{1}{2}d_{b,k}, \frac{1}{2}d_{b,k})$. While tracking the bubble movement with respect to the probe, a synthetic signal time series is recorded for each sensor of the virtual phase-detection probe, with the signal taking values of 1 if the sensor lies inside the bubble and 0 otherwise. The bubble movement is tracked at a sampling frequency f_s of 500 kHz, which corresponds to typical sampling frequencies of dual-tip probes (e.g., Felder and Pfister, 2017; Felder et al., 2019). Therefore, the bubble trajectory obtained through Eq. [4] was interpolated linearly between time steps Δt_1 to match the tracking time step $\Delta t_2 = 1/f_s$, corresponding to the sampling frequency f_s of the probe. Effects of bubble-probe interaction, such as deformation, deflection, or deceleration of the bubble, are neglected (Hohermuth et al., 2021). An example of synthetic signals generated by a with a 4-sensor probe is illustrated in Figure 3.

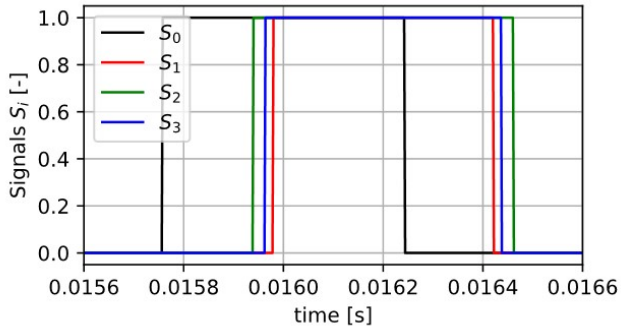

Figure 3. Exemplary short sequence of a synthetic signal time series of the four sensors S_0 to S_3.

2.3 Signal Processing Algorithms

Three different signal processing algorithms for measuring local flow properties are compared in this study, one for dual-tip and two for 4-sensor phase-detection intrusive probes. For the dual-tip probes, the adaptive window cross-correlation (AWCC) technique was applied as described by Kramer et al. (2019, 2020a). The AWCC technique measures the local pseudo-instantaneous 1-D velocity, whereas each velocity estimation corresponds to a small group of bubbles. The number of bubbles per averaging window N_p was varied with 5, 10 and 15, covering the range recommended by Kramer et al. (2020a). For the cross-correlation based filtering, a threshold value $A = 0.4$ was selected, following the recommendations of Kramer et al. (2020a). Further, the measured velocity time series was filtered iteratively until no more outliers were rejected, using a robust outlier cutoff (ROC) filter based on the median (MED) and the median absolute deviation from the median (MAD) as estimators of location and scale (Valero et al., 2020). The threshold, for which a velocity value is rejected, is defined according to Valero et al. (2020) as $\delta_{ROC} = \lambda_n q\, MAD$, with $\lambda_n = \sqrt{2\ln(N)}$ being the universal threshold (Goring and Nikora, 2002), N being the number of velocity values in the reconstructed time series, q being the coefficient relating the MAD to the standard deviation, taking a value of q = 1.483 (Rousseeuw and Croux, 1993). Rejected values were replaced by NaN values (standing for Not a Number). The effect of ROC filtering on the velocity histogram is demonstrated in Figure 4a. Bubble diameters were calculated from measured chord lengths L_{ch} as $d_b = 3/2L_{ch}$ (Chanson, 2002).

For four-sensor probes, the signal processing algorithms of Shen and Nakamura (2014) and of Tian et al. (2015) were compared. Both algorithms are based on event detection and require an interface-paring signal processing scheme as a pre-processing step to identify the corresponding signals for the same interface detected by different sensors of the four-sensor probe. In this study, the interface-pairing algorithm proposed by Shen et al. (2005) was applied. Since this interface-pairing algorithm requires a rough initial estimate of the velocity, we applied the AWCC technique using the signals of the leading sensor and the trailing sensor with the shortest lateral separation to obtain an estimate of the mean velocity. Both algorithms make use of the geometric configuration of the four-sensor probe as well as the three time differences $\Delta t_{0,l} = t_l - t_0$, between the times at which a bubble interface is registered by the leading sensor (t_0) and by each of the trailing sensors

t_l (for l = 1, 2, 3), respectively. While the algorithm of Shen and Nakamura (2014) assumes spherical bubbles, the algorithm of Tian et al. (2015) does not rely on assumptions regarding the bubble shape. By making an assumption on the bubble shape, the algorithm of Shen and Nakamura (2014) is also capable of retrieving bubble diameters in addition to the 3-D interfacial velocity vector.

The signal processing algorithms of Shen and Nakamura (2014) and of Tian et al. (2015) have predominantly been applied to flow with both small void fractions and flow velocities, since event detection techniques aim at identifying isolated, individual bubbles. In flows with high air concentrations in combination with relatively small bubbles, i.e., bubble dimensions in the same order as the phase-detection probe size, we found that falsely paired interface detections can lead to significant under- or overestimations of instantaneous velocities. Depending on the simulated bubble size distribution, velocity measurements from falsely paired interface detections accounted for more than half of the values of the measured velocity time series. Further, we observed that underestimations of instantaneous velocities occurred more frequently than overestimations, resulting in asymmetrical, multimodal distributions around the true mean velocity. Hence, a robust filtering approach is necessary to remove velocities from falsely paired interface detections. However, a filter such as ROC based on robust estimators, i.e., MED and MAD, have a breakdown point of 50% (Valero et al., 2020) and thus might fail, especially for multimodal distributions.

Therefore, we include an additional filtering step before ROC filtering, based on a modification of the robust outlier cutoff filter to include prior knowledge. More specifically, we approximate the location with the time averaged velocity obtained from AWCC. Further, the median absolute deviation is replaced by the RMS velocity obtained from AWCC processing, resulting in a rejection threshold of $\delta_{FLT} = \lambda_n u_{rms,AWCC}$. The effect of pre-filtering (FLT) based on mean and RMS velocity from AWCC prior to ROC filtering is demonstrated in Figure 4b. Note that standard ROC filtering was applied, too, after FLT.

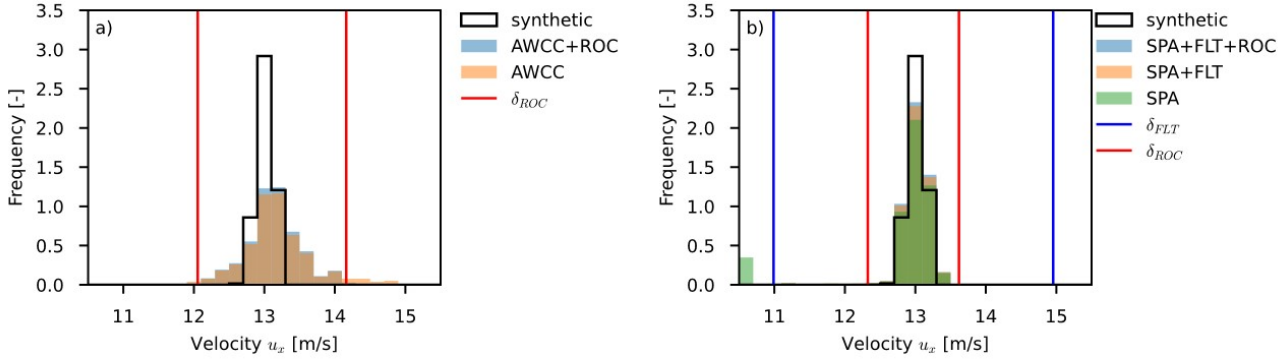

Figure 4. Effect of a) ROC filtering of a velocity time series measured with AWCC and b) filtering (FLT) a velocity time series measured with the signal processing (SPA) algorithm of Shen & Nakamura (2014) based on mean and root mean square velocities from AWCC before ROC filtering.

3. APPLICATION TO AERATED UNIFORM FLOW ON A SPILLWAY CHUTE

Synthetic signals were generated at different vertical locations above the invert of a spillway flume with aerated uniform flow. The spillway chute was assumed with an angle of θ = 45° and a surface roughness of 1 mm. For a specific discharge of 0.3 m²/s, uniform clear water depth h_w = 0.044 m and depth averaged flow velocity U =13.6 m/s were calculated iteratively using the Colebrook-White equation (Colebrook and White, 1937), while taking into account the friction reduction due to entrained air (Chanson, 1996). The mean air concentration over the depth was calculated as $C_m = 0.75\sin(\theta)^{0.75} = 0.578$ (Hager, 1991) and the mixture flow depth as $h_{90} = \frac{h_w}{1-C_m}$ = 0.104 m. Further, the vertical profile of the time-averaged, streamwise flow velocity $\bar{u}_f$ was obtained assuming a power-law with n = 6 (Chanson, 1996) given by,

$$\bar{u}_f(z) = \bar{u}_{f_{90}} \left(\frac{z}{h_{90}}\right)^{1/n} \quad [5]$$

where $\bar{u}_{f_{90}}$ is the time averaged flow velocity at $z = h_{90}$, and z is the distance from the invert perpendicular to the chute. Spanwise and wall-normal time averaged velocities were assumed as zero. The streamwise RMS velocity fluctuations were approximated by an empirical relation for non-aerated chute flow as $u'_{f,x,rms}(z) = 2.3u^* e^{(-z/h)}$ (Nezu and Nakagawa 1993), where u^* is the shear velocity and h was replaced by the mixture flow depth h_{90}. The spanwise and wall-normal RMS velocity fluctuations were approximated as half of streamwise RMS velocity fluctuations, respectively. This is in agreement with data from direct numerical simulations of boundary layer flows (Kim et al., 1987; Pope, 2000). The streamwise integral time scale was approximated as

$T_{L,x} \approx h/\bar{u}_f(z)$ as in Valero et al. (2019), while the spanwise and wall-normal integral time scales were again approximated as half of the integral time scale (Pope, 2000), respectively. In contrast to Valero et al. (2019), shearing was accounted for by drawing ξ from a multivariate Gaussian distribution with a covariance between the x and z component of −0.45. The integration time step of the Langevin equation (Eq. [2]) was defined as $\Delta t_1 = \frac{T_{L,x}}{50}$, following the recommendation that the time integration time step should be larger than the Kolmogorov time scale, but smaller than the integral time scale (Pope, 2000).

The vertical air concentration distribution was calculated according to Eq. [6] (Chanson, 1996), where $\mathcal{K}$ is an integration constant. The dimensionless diffusivity D' can be derived from the mean air concentration C_m.

$$C_a(z) = 1 - tanh^2\left(\mathcal{K} - \frac{z}{2D'}\right)^{1/n} \quad [6]$$

Further, the vertical distribution of the mean bubble diameter was approximated by Eq. [7], based on considerations of the critical bubble size before splitting due to shear stresses occurs (Hinze, 1955) and based on the assumption of a power law velocity distribution with n = 6. A critical Weber number of We_c = 1 results in good agreement with experimental results (Chanson, 1993) and was chosen herein. The surface tension between air and water is denoted as σ_{aw}.

$$d_b(z) = \sqrt[3]{2n^2 \frac{We_c \sigma_{aw}}{\rho_f U_{90}^2 h_{90}} \left(\frac{z}{h_{90}}\right)^{2(n-1)/n}} \quad [7]$$

The resulting normalized vertical profiles of the streamwise time-averaged and root mean fluctuating velocities, the air concentration, and the mean bubble diameter are shown in Figure 5.

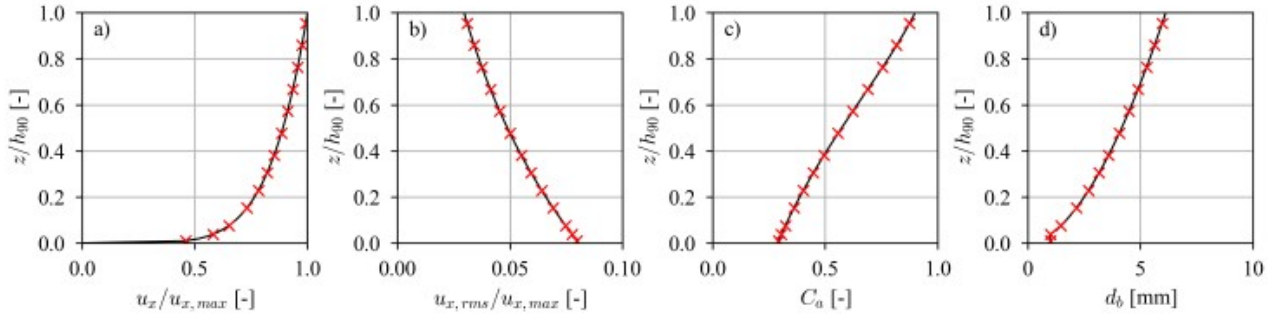

Figure 5. Normalized vertical profiles of the a) streamwise time-averaged and b) root mean fluctuating velocity, c) air concentration and d) mean bubble diameter. The red crosses mark the vertical discretization.

Stochastic time series were generated for 13 locations in vertical direction (red crosses in Fig. 5). The duration of the stochastic time series was determined such that at least 2000 bubbles were pierced by all sensors of each probe, respectively. Two virtual probe designs were used to generate the synthetic signals, one dual-tip and one four-sensor phase-detection probe. The design of the virtual dual-tip phase-detection was characterized by separation in streamwise and transverse directions by Δx = 5.06 mm and Δy = 0.97 mm. A probe with similar dimensions was used for example by Felder and Pfister (2017) and Hohermuth et al. (2021). For the four-sensor probe the geometrical configuration described in Shen et al. (2005) at a relative pipe length of 11.4 was adopted. The tips of the probes were idealized as discrete point locations. Finally, the signal processing algorithms described in Section 2.3 were applied to retrieve flow properties.

4. RESULTS AND DISCUSSION

The reconstructed flow properties are illustrated in Figure 6 as vertical profiles. For the considered test case, the signal processing algorithms of Shen and Nakamura (2014) and Tian et al. (2015) resulted in identical instantaneous velocities, turbulent statistics, and data rates. A detailed comparison revealed that both algorithms are derived from similar concepts, with the main difference that Tian et al. (2015) assume a bubble to have a plane of symmetry normal to the direction of motion, while Shen and Nakamura (2014) assume spherical bubbles. Accounting for the fact that we only simulate spherical bubbles, the identical velocity results are thus not surprising. For the sake of conciseness, the algorithm of Tian et al. (2015) is therefore not discussed in detail in the following.

All considered signal processing algorithms provide almost identical time-averaged flow velocities (Fig. 6a), which agree with the time-averaged velocities of the stochastic time series of the dispersed phase (±2.7 % max. deviation).

Close to the invert, mean bubble diameters resulting with the algorithm of Shen and Nakamura (2014) are slightly larger than those obtained with AWCC, while for z/h_{90} > 0.3, the latter results in larger bubbles (Fig 6b). In comparison to the mean diameters used for the signal generation, both algorithms result in a significant overestimation of the bubble diameter. Both, the dual-tip as well as the four-sensor probe exhibit lateral dimension in the order of 1 mm. Bubbles with diameters smaller than 1 mm are often missed by one or more sensors of the four-sensor probe, resulting in the significant overestimation especially close to the invert, where the number of bubbles <1 mm is substantial. Thus, reducing the spatial dimensions of the four-sensor probes could improve measurements of the mean bubble size. The algorithm of Tian at al. (2015) does not propose any relation to recover the bubble diameter and is therefore not included in Figure 6b. The generation of synthetic signal assumes that air transport occurs in the form of dispersed bubbles in a water body (entrained air), which is an adequate assumption for a large part of the water column of aerated free-surface flows. However, close to the free-surface the flow regime is more accurately described by entrapped air pockets between surface waves (Wilhelms and Gulliver, 2005) and droplets (Killen, 1968). Measurements of Bung (2013) suggest that entrapped air becomes relevant above $z/h_{90} \approx 0.75$. Therefore, the bubble diameters used in the upper part of the flow are likely not representative of the true flow regime.

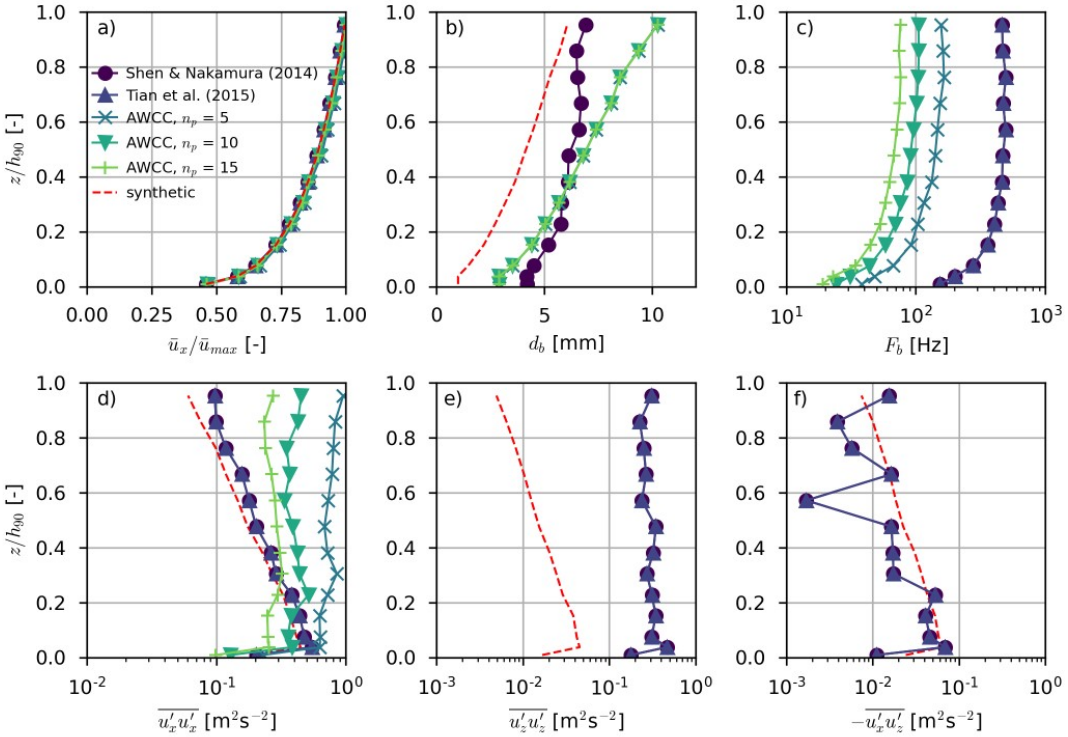

Figure 6. Vertical profiles of the a) mean streamwise velocities, b) mean bubble diameter, c) bubble count rate, d) streamwise normal stresses, e) wall-normal stresses, and f) shear stresses of the streamwise and wall-normal components.

As evident from Figure 6c, the data rates F_b resulting with Shen and Nakamura (2014) are significantly larger than those obtained with AWCC. On average, we found an increase in data rate by a factor of five in comparison to AWCC with N_p = 10. In contrast, Kramer et al. (2020b) only observed a doubling of the data rate for an event detection based algorithm for dual-tip probes, which was applied to a signal dataset of a stepped spillway. The differences are likely due to the larger lateral size of the probe used by Kramer et al. (2020b), or due to differences in bubble size. The larger data rate constitutes a significant advantage of using four-sensor probes with event-detection based signal processing algorithms for the retrieval of time-resolved turbulence statistics. The data rate from AWCC processing can be increased by reducing the number of particles per averaging window, but at the cost of larger errors in measuring the streamwise normal stresses (Fig. 6d).

Turbulent normal and shear stresses of the streamwise and wall-normal components play an important role in the entrainment and transport of air in free-surface flows on spillways (e.g., Chanson, 2009) and are therefore of particular interest. The results in Figure 6d suggest, that a four-sensor probe in combination with the signal processing algorithm of Shen and Nakamura (2014) can significantly improve measurements of streamwise normal stresses in comparison to AWCC. For relative depths larger than 0.5, the measured normal stresses exhibit slightly larger deviations from the stresses of the stochastic time series. We found that two factors contribute to the increasing deviation towards the free surface: the increasing velocity and increasing air

concentration. The algorithm of Shen and Nakamura (2014) relies on the time differences between the interface detection of leading and trailing sensors. The error in measuring these time differences increases with increasing velocity because the sensors only have a finite sampling frequency. Therefore, increasing measurement errors for the instantaneous velocity are expected for larger flow velocities, but could be compensated by increasing the sampling frequency of the sensors. Evaluating the sensitivity with regard to the sampling frequency and velocity could be subject of future research. Further, we found that with increasing air concentration, the number of falsely paired interface detections increased, which can lead to significant under- or overestimations of instantaneous velocities and therefore to overestimation of turbulent fluctuations. While appropriate filtering significantly reduced errors of the measured turbulent stresses, some errors remained. Improved filtering criteria could be subject to future research. As evident from Figure 6e, the measured normal stresses of the wall-normal components exhibit significant deviations from those of the stochastic time series. The reconstruction of wall-normal and spanwise velocity components is based on variations between the three measured time difference $\Delta t_{0,l}$. For the underlying test case, the mean streamwise flow velocity is approximately one order of magnitude larger than the wall-normal and spanwise RMS velocity fluctuations. This caused the variations between the three time differences $\Delta t_{0,l}$ to be of similar order of magnitude as the error resulting due to the finite sampling frequency and ultimately resulted in significant errors when reconstructing the normal and spanwise velocity components. Therefore, we expect, that the measurement accuracy of normal stresses of the wall-normal components could be improved by increasing the sampling frequency of the sensors. The shear stresses formed by the streamwise and wall-normal components are in reasonable agreement with those of the stochastic time series, but occasionally show larger deviations above z/h_{90} > 0.5 (cf. Figure 6f). We recommend to be cautious with the results for z/h_{90} > 0.7 in Figure 6 for two reasons. First, it can be shown that bubbles begin to overlap for air concentrations $C_a > 0.67$, assuming a 1-D stream of bubbles. Thus, simulating air concentrations exceeding that threshold may result in a non-physical overlap of subsequent bubbles. Second, the followed approach of simulating the motion of individual bubbles may not be sufficiently representative of the flow regime in the vicinity of the free-surface described as “bubbles and waves” by Wilhelms and Gulliver (2005). Therefore, air-concentrations of $C_a \approx 0.67$ should be regarded as the upper practical limit for the underlying approach of synthetic signal generation. For larger air concentrations, validation based on signals measured in physical experiments seems unavoidable.

Our results suggest that the use of four-sensor intrusive phase-detection probes in combination with event detection based signal processing algorithms can significantly improve measurement accuracy for streamwise time-resolving turbulent statistics in highly turbulent, aerated free-surface flows in comparison to the current best practice with dual-tip probes and AWCC signal processing. Additionally, the measurement of shear stresses could improve our understanding of air entrainment and transport processes. Further, data rates can be increased by roughly one order of magnitude. The algorithm of Shen & Nakamura (2014) has the advantage of also providing information on the bubble diameters. Whether the algorithm of Tian et al. (2015) can provide more accurate measurements in flow with non-spherical bubbles should be subject of future studies.

5. CONCLUSIONS

In this study we compare the two signal processing algorithms of Shen & Nakamura (2014) and Tian et al. (2015) for four-sensor intrusive phase-detection probes by making use of synthetically generated signals of aerated uniform flow on a spillway. A dual-tip probe with AWCC signal processing, which currently represents the best practice in the field of hydraulic engineering, was used as a benchmark. For spherical bubbles, the algorithms of Shen & Nakamura (2014) and Tian et al. (2015) resulted in identical reconstructed instantaneous velocity time series. We found that both algorithms for four-sensor probes resulted in identical mean velocities as the AWCC algorithm, while retrieving streamwise normal stresses with significantly improved accuracy compared to the AWCC algorithm. Further, the bubble count rate could be increased on average by a factor of five. Bubble diameters were significantly overestimated by the algorithm of Shen and Nakamura (2014), but also with AWCC, since bubbles smaller than ~1 mm were mostly missed by the probes. Air concentrations of $C_a \approx 0.67$ represent an upper practical limit for the followed approach for synthetic signal generation and results for relative depths z/h_{90} > 0.7 should be regarded with caution. Further, we found that robust filtering is necessary to improve the velocity estimation. Future research could focus on investigating the performance for non-spherical bubbles, uncertainty quantification related to the sampling frequency of four-sensor probes and optimization of the 4-tip sensor geometry.

6. ACKNOWLEDGEMENTS

The first and second author were supported by the Swiss National Science Foundation (SNSF) [grant number 197208]. The fruitful discussion with Dr. Stefan Felder (UNSW) and Dr. Daniel Valero (KIT) are gratefully acknowledged.

7. REFERENCES

Aberle, J., Rennie, C.D., Admiraal, D.M., and Muste, M. (2017). Experimental Hydraulics: Methods, Instrumentation, Data Processing and Management: Volume II: Instrumentation and Measurement Techniques. *CRC Press*.

Balachandar, S., and Eaton, J.K. (2010). Turbulent dispersed multiphase flow. *Annual Review of Fluid Mechanics*, 42, 111-133.

Bauer, W.J. (1954). Turbulent boundary layer on steep slopes. *Transactions of the American Society of Civil Engineers*, 119(1), 1212-1233.

Boes, R.M., and Hager, W.H. (2003). Two-phase flow characteristics of stepped spillways. *Journal of Hydraulic Engineering*, 129(9), 661-670.

Cain, P. (1978). Measurements within self-aerated flow on a large spillway. *PhD thesis*, Univ. of Canterbury, Christchurch, New Zealand.

Cain, P., and Wood, I.R. (1981). Measurements of self-aerated flow on a spillway. *Journal of Hydraulic Division* 107 (11), 1425–1444.

Castro-Orgaz, O., and Hager, W.H. (2010). Drawdown curve and turbulent boundary layer development for chute flow. *Journal of Hydraulic Research*, 48(5), 591-602.

Chanson, H. (1994). Drag reduction in open channel flow by aeration and suspended load. *Journal of Hydraulic Research*, 32(1), 87-101.

Chanson, H. (1997). Air bubble entrainment in open channels: flow structure and bubble size distributions. *International Journal of Multiphase Flow*, 23(1), 193-203.

Chanson, H. (1996). Air bubble entrainment in free-surface turbulent shear flows. Elsevier.

Chanson, H. (1997). Air bubble entrainment in open channels: flow structure and bubble size distributions. *International Journal of Multiphase Flow*, 23(1), 193-203.

Chanson, H. (2002). Air-water flow measurements with intrusive, phase-detection probes: Can we improve their interpretation?. *Journal of Hydraulic Engineering*, 128(3), 252-255.

Chanson, H. (2009). Turbulent air-water flows in hydraulic structures: dynamic similarity and scale effects. *Environ. Fluid Mech*. 9 (2), 125–142.

Chanson, H. (2013). Hydraulics of aerated flows: qui pro quo?. *Journal of Hydraulic Research*, 51(3), 223-243.

Chanson, H. (2016). Phase-detection measurements in free-surface turbulent shear flows. *Journal of Geophysics and Engineering*, 13(2), S74-S87.

Chanson, H., and Toombes, L. (2002). Air-water flows down stepped chutes: turbulence and flow structure observations. *International Journal of Multiphase Flow*, 28(11), 1737-1761.

Colebrook, C. F. and White, C. M. (1937). "Experiments with Fluid Friction in Roughened Pipes". Proceedings of the Royal Society of London. Series A, *Mathematical and Physical Sciences*. 161 (906): 367–381.

Crowe, C., Sommerfeld, M., Tsuji, Y., and Crowe, C. (1998). Multiphase Flows with Droplets and Particles CRC. Boca Raton, FL.

Ervine, D.A., and Falvey, H.T. (1987). Behaviour of turbulent water jets in the atmosphere and in plunge pools. *Proceedings of the Institution of Civil engineers*, 83(1), 295-314.

Felder, S., and Chanson, H. (2014). Air–water flows and free-surface profiles on a non-uniform stepped chute. *Journal of Hydraulic Research*, 52(2), 253-263.

Felder, S., and Chanson, H. (2015). Phase-detection probe measurements in high-velocity free-surface flows including a discussion of key sampling parameters. *Experimental Thermal and Fluid Science*, 61, 66-78.

Felder, S., Hohermuth, B., and Boes, R.M. (2019). High-velocity air-water flows down-stream of sluice gates including selection of optimum phase-detection probe. *International Journal of Multiphase Flow* 116, 203–220.

Felder, S., and Pfister, M. (2017). Comparative analyses of phase-detective intrusive probes in high-velocity air-water flows. *International Journal of Multiphase Flow* 90, 88–101.

Hager, W.H. (1991). Uniform aerated chute flow. *Journal of Hydraulic Engineering*, 117(4), 528-533.

Hinze, J.O. (1955). Fundamentals of the hydrodynamic mechanism of splitting in dispersion processes. *AIChE Journal*, 1(3), 289-295.

Hohermuth, B., Kramer, M., Felder, S., and Valero, D. (2021). Velocity bias in intrusive gas-liquid flow measurements. *Nature Communications*, 12(1), 1-9.

Killen, J.M. (1968). The surface characteristics of self aerated flow in steep channels. *PhD thesis,* University of Minnesota, Minneapolis, USA.

Kim, J., Moin, P., and Moser, R. (1987). Turbulence statistics in fully developed channel flow at low Reynolds number. *Journal of Fluid Mechanics*, 177, 133-166.

Kramer, M. (2019). Particle size distributions in turbulent air-water flows. In *E-Proceedings of the 38th IAHR World Congress* (pp. 5722-5731).

Kramer, M., Valero, D., Chanson, H., and Bung, D.B. (2019). Towards reliable turbulence estimations with phase-detection probes: an adaptive window cross-correlation technique. *Experiments in Fluids*, 60(1), 1-6.

Kramer, M., Hohermuth, B., Valero, D., and Felder, S. (2020a). Best practices for velocity estimations in highly aerated flows with dual-tip phase-detection probes. *International Journal of Multiphase Flow*, 126, 103228.

Kramer, M., Hohermuth, B., Valero, D., and Felder, S. (2020b). Leveraging event detection techniques and cross-correlation analysis for phase-detection probe measurements in turbulent air-water flows. *8th IAHR International Symposium on Hydraulic Structures ISHS2020,* Santiago, Chile, 12-15 May 2020.

Neal, L.G., and Bankoff, S.G. (1963). A high resolution resistivity probe for determination of local void properties in gas-liquid flow. *AIChE Journal*, 9(4), 490-494.

Nezu, I., and Nakagawa, H. (1993). Turbulence in open-channel flows. *IAHR monograph*, Balkema, Rotterdam, The Netherlands

Pope, S.B. (2000). Turbulent flows. *Cambridge university press*.

Rousseeuw, P.J., and Croux, C. (1993). Alternatives to the median absolute deviation, *J. Am.Stat. Assoc*. 88 (424) 1273–1283

Shen, X., Saito, Y., Mishima, K., and Nakamura, H. (2005). Methodological improvement of an intrusive four-sensor probe for the multi-dimensional two-phase flow measurement. *International Journal of Multiphase Flow*, 31(5), 593-617.

Shen, X., and Nakamura, H. (2014). Spherical-bubble-based four-sensor probe signal processing algorithm for two-phase flow measurement. *International Journal of Multiphase Flow*, 60, 11-29.

Straub, L.G., and Anderson, A.G. (1958). Experiments on self-aerated flow in open channels. *Journal of the Hydraulics Division*, 84(7), 1-35.

Tian, D., Yan, C., and Sun, L. (2015). Model of bubble velocity vector measurement in upward and downward bubbly two-phase flows using a four-sensor optical probe. *Progress in Nuclear Energy*, 78, 110-120.

Tomiyama, A., Kataoka, I., Zun, I., and Sakaguchi, T. (1998). Drag coefficients of single bubbles under normal and micro gravity conditions. *JSME International Journal Series B Fluids and Thermal Engineering*, 41(2), 472-479.

Valero, D., Kramer, M., Bung, D.B., and Chanson, H. (2019). A stochastic bubble generator for air water flow research. In *E-Proceedings of the 38th IAHR World Congress*. Panama City, Panama, pp. 5714–5721.

Valero, D., Chanson, H., and Bung, D.B. (2020). Robust estimators for free surface turbulence characterization: A stepped spillway application. *Flow Measurement and Instrumentation*, 76, 101809.

Wahl, T.L. (2003). Discussion of “Despiking acoustic doppler velocimeter data” by Derek G. Goring and Vladimir I. Nikora. *Journal of Hydraulic Engineering*, 129(6), 484-487.

Welch, P. (1967). The use of fast Fourier transform for the estimation of power spectra: a method based on time averaging over short, modified periodograms. *IEEE Transactions on audio and electroacoustics*, 15(2), 70-73.

Wilhelms, S.C., and Gulliver, J.S. (2005). Bubbles and waves description of self-aerated spillway flow. *Journal of Hydraulic Research*, 43(5), 522-531.

Wood, I.R. (1983). Uniform region of self-aerated flow. *Journal of Hydraulic Engineering*, 109(3), 447-461.

Wood, I.R. (1991). Air Entrainment in Free-Surface Flows. *IAHR Hydraulic Structures Design Manual No. 4, Hydraulic Design Considerations*, Balkema, Rotterdam, The Netherlands, 149 pages.